Journal of Inflammation Research

Dovepress
Taylor & Francis Group

Open Access Full Text Article

ORIGINAL RESEARCH

Chinese Massage (Tuina) Attenuates Knee Osteoarthritis by Modulating Autophagy-Related Cytokines: A Multidisciplinary Methodological Investigation

Zhen Wang[1,*], Chi Zhao[1,2,*], Mengmeng Li[1,2,*], Lili Zhang[1,*], Jieyao Diao[1], Yiming Wu[2], Tao Yang[2], Mingwei Shi[2], Yang Lei[2], Yu Wang[3], Miaoxiu Li[4], Yanqin Bian[5], Yunfeng Zhou[1], Hui Xu[1,2]

[1]College of Acupuncture and Massage, Henan University of Chinese Medicine, Zhengzhou, People's Republic of China; [2]Acupuncture and Massage Department, The Third Affiliated Hospital of Henan University of Chinese Medicine, Zhengzhou, People's Republic of China; [3]College of Computer Science, Xidian University, Xian, People's Republic of China; [4]College of Acupuncture and Massage, Shanghai University of Chinese Medicine, Shanghai, People's Republic of China; [5]Orthopaedic Research Laboratory, University of California, Davis, CA, USA

*These authors contributed equally to this work

Correspondence: Hui Xu, Email 15036065036@163.com

Background: Tuina therapy has demonstrated its potential in modulating autophagy-related factors in knee osteoarthritis (KOA); however, its core therapeutic targets and specific mechanisms require systematic elucidation through interdisciplinary research.

Objective: This study investigated the mechanism by which Tuina alleviates KOA progression using multidimensional approaches, including Mendelian randomization (MR), in vivo experiments, and machine learning.

Methods: Genetic data from genome-wide association studies of 60 cytokines and KOA were analyzed using MR analysis to identify autophagy-related factors significantly associated with KOA. A KOA rat model was established via intra-articular injections of L-cysteine–activated papain solution into the right knee. The key autophagy-related cytokines identified by MR were validated using enzyme-linked immunosorbent assay (ELISA). Cartilage degeneration and autophagic activity were assessed through histological evaluation via safranin O/fast green (SO/FG) staining and ultrastructural analysis via transmission electron microscopy (TEM). A Support Vector Machine (SVM) algorithm was used to conduct a secondary analysis of the experimental dataset to predict comprehensive therapeutic effects and synergistic correlations among the indicators.

Results: MR analysis revealed causal relationships between eight cytokines and KOA at genetically determined levels, with seven exhibiting autophagy-related regulatory properties. Tuina significantly alleviated pain and improved motor function. SO/FG staining and TEM revealed reduced cartilage destruction, increased cartilage thickness, and decreased chondrocyte autophagy. ELISA revealed that Tuina downregulated interferon gamma, parathyroid hormone, interleukin (IL)–1β, matrix metalloproteinase-3, and IL-17 levels in the cartilage while upregulating osteocalcin and transforming growth factor-β1 levels. Furthermore, Tuina demonstrated superior comprehensive and classified curative effects compared with celecoxib. IFN-γ and PTH were strongly correlated with both relative autophagy level and cartilage area ratio. Autophagy-related cytokines had the strongest correlation with the degree of cartilage degeneration.

Conclusion: Tuina therapy alleviates pain and functional impairment in KOA by suppressing chondrocyte autophagy and delaying cartilage degeneration. This mechanism may involve the regulation of autophagy-related cytokines.

Keywords: knee osteoarthritis, autophagy-related cytokines, Tuina, Mendelian randomization, in vivo experiment, machine learning

Introduction

Knee osteoarthritis (KOA), characterized primarily by the degenerative deterioration of the articular cartilage, manifests clinically through symptoms such as persistent knee pain, joint stiffness, and restricted range of motion, significantly impairing patients' quality of life.[1,2] Epidemiological data revealed a global increase of 48% in the prevalence of KOA between 1990

Received: 26 May 2025
Accepted: 23 July 2025
Published: 2 August 2025

and 2019, establishing it as a growing public health challenge.[3] Current therapeutic approaches include non-surgical options such as medication, laser therapy, acupoint injection, and various surgical interventions, including arthroscopic debridement, high-tibial osteotomy, and single-compartment knee arthroplasty.[4–8] Although these modalities demonstrate varying degrees of clinical efficacy, they have notable limitations, including substantial treatment costs, plateaued therapeutic outcomes, significant adverse effects, and unclear mechanisms of action.[9] Consequently, there is an urgent need to identify novel therapeutic targets and nonpharmacological strategies capable of mitigating disease progression.

Emerging evidence has implicated dysregulated cellular autophagy as a pivotal contributor to KOA pathogenesis. Autophagy, a conserved lysosomal degradation pathway, maintains chondrocyte homeostasis by clearing damaged organelles and protein aggregates under physiological conditions.[10,11] However, an excessive or impaired autophagic flux disrupts the cartilage matrix metabolism, exacerbates oxidative stress, and accelerates chondrocyte apoptosis, thereby promoting cartilage degeneration. Key cytokines, including interleukin-1β (IL-1β), matrix metalloproteinase-3 (MMP-3), and transforming growth factor-β1 (TGF-β1), have been identified as critical regulators of autophagy–chondrocyte crosstalk in KOA.[12–14] Despite these advances, the precise regulatory network linking autophagy-related cytokines to KOA progression remains poorly characterized, hindering the development of targeted therapies.

Chinese massage therapy (Tuina) represents an integrative manual intervention combining biomechanical stimulation and neuroregulation.[15,16] Recognized for its multi-target regulatory capacity, clinical efficacy, and favorable safety profile, this modality has emerged as a valuable therapeutic approach for KOA. Our previous clinical investigations demonstrated the effectiveness of Tuina in elevating pressure pain thresholds, alleviating discomfort, and restoring functional capacity.[17–19] However, the mechanism of action of Tuina in KOA remains unclear, necessitating further empirical investigation. Emerging evidence suggests that Tuina exerts chondroprotective effects through the modulation of autophagy mediated by cytokine regulation and metabolic reprogramming of chondrocytes. Mechanistic investigations have proposed that Tuina-induced release of IL-1β from local tissues may suppress excessive autophagy (thereby, preventing abnormal chondrocyte death) via ERK1/2-NF-κB pathway inhibition.[20] Furthermore, Tuina appears to upregulate TGF-β1 expression, restore MMP-3/tissue inhibitor of metalloproteinase-1 balance, and regulate the balance of autophagy–anabolic processes, potentially decelerating cartilage degeneration.[21]

However, these experimental studies present significant methodological challenges. Multidimensional confounding factors, including environmental conditions, lifestyle variations, and dietary habits, complicate mechanistic interpretation.[22] Current research paradigms exhibit limitations in biomarker selection, often relying on investigator subjectivity or literature-derived assumptions rather than systematic screening of the extensive autophagy-related cytokine network.[23] Moreover, conventional experimental designs that focus on isolated outcome measures fail to capture the holistic regulatory effects and interdependent relationships among biological markers, thereby constraining the generalizability of the findings and impeding a comprehensive understanding of Tuina's therapeutic network.

Mendelian randomization (MR), an emerging paradigm in genetic epidemiology, has revolutionized causal inferences in experimental studies by leveraging genetic variations as instrumental variables.[24] This innovative approach effectively addresses the persistent limitations of traditional experimental research by minimizing interference from environmental confounders and circumventing misleading conclusions caused by reverse causality, thereby significantly enhancing the validity of causal mechanism exploration in complex diseases. MR integrates theoretical frameworks from population genetics and causal inference to systematically analyze genetic-level causal relationships between phenotypes.[25,26] Disease-associated biomarkers identified through MR studies demonstrate not only statistical significance but also biological plausibility, offering genetically validated high-value therapeutic targets for experimental investigations. Machine learning (ML), empowered by its robust data processing and pattern recognition capabilities, enables the predictive analysis of intricate biological datasets.[27] It transcends the analytical constraints of conventional statistical methods in deciphering complex relationships while addressing the challenges in data interpretation and outcome prediction inherent to experimental studies. Furthermore, machine learning facilitates the elucidation of synergistic interaction networks among biological indicators and enables the prediction of comprehensive therapeutic effects of intervention strategies.[28]

This study employed an interdisciplinary framework integrating MR, in vivo rat experiments, and ML to systematically elucidate the regulatory mechanisms of autophagy-related cytokines by Tuina for KOA. Our approach involves

three systematic stages: First, MR analysis was performed to identify autophagy-related cytokines that are closely related to KOA at the genetic level. Second, autophagy-related cytokines identified by MR were verified using the rat KOA model. Third, multimodal data integration using ML algorithms was performed to quantify synergistic interactions and establish predictive models for therapeutic outcomes. This multimodal approach aimed to establish quantitative evidence for the multitarget synergistic mechanism of Tuina intervention in KOA.

Materials and Methods

The technical route of this study is shown in Figure 1, and the specific implementation process is divided into three progressive stages: first, based on the bidirectional two-sample MR analysis method, autophagy-related cytokines with a significant causal association with KOA at the genetic level were systematically screened. Next, through the experimental rat models in vivo, the key autophagy-related cytokines identified by MR were detected by enzyme-linked immunosorbent assay (ELISA), combined with transmission electron microscopy (TEM), behavior detection, and safranin O/fast green (SO/FG) staining of the cartilage tissue, to systematically analyze the potential mechanism of Tuina intervention in KOA. Finally, ML was used to deeply examine the experimental dataset, and the core findings of MR analysis and in vivo experiments were further verified and improved by constructing a support vector machine (SVM) prediction model.

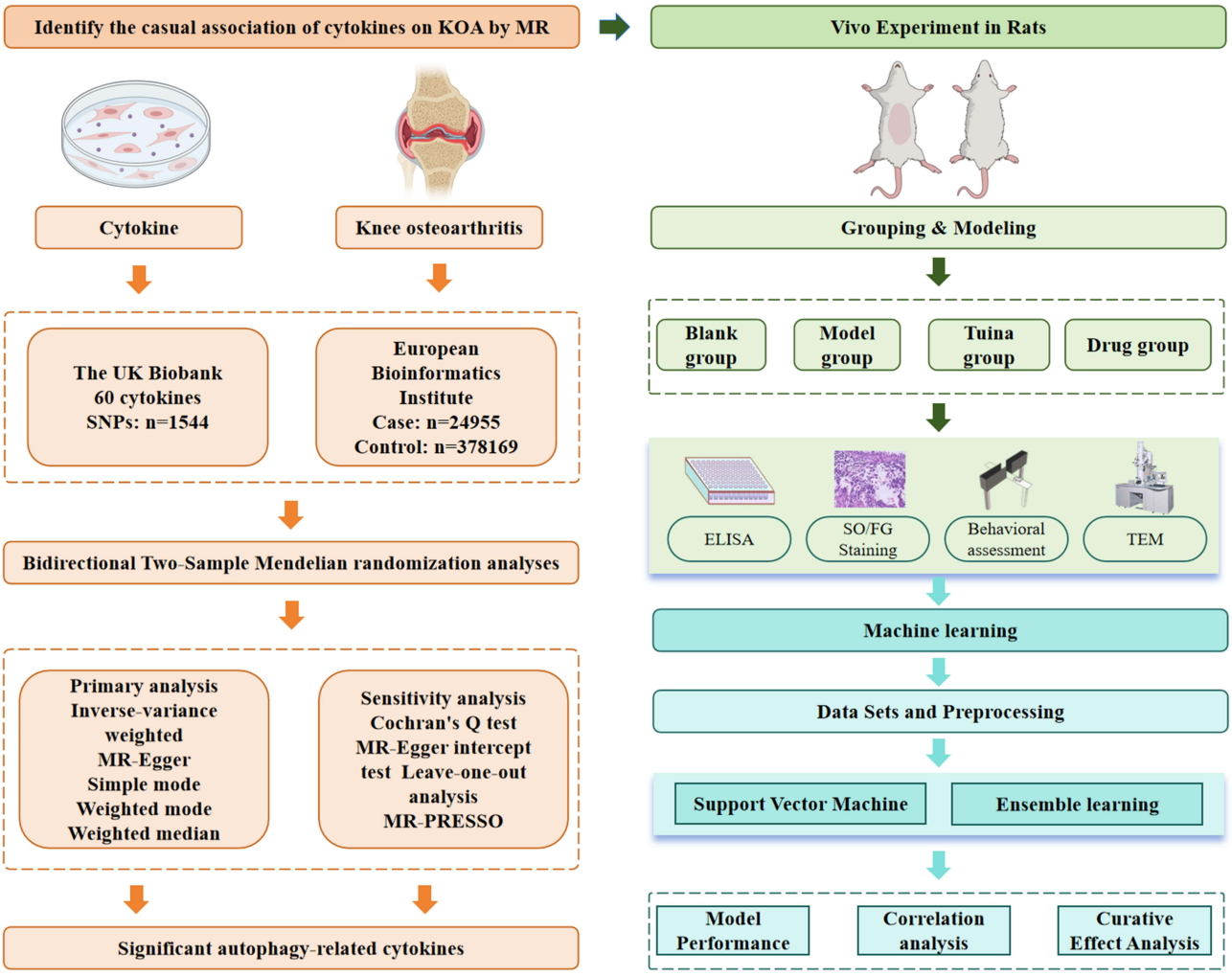

Figure 1 Overview technical route of the study design.
Abbreviations: MR, Mendelian randomization; KOA, knee osteoarthritis; SNPs, single nucleotide polymorphisms; PRESSO, pleiotropy residual sum and outlier; ELISA, enzyme-linked immunosorbent assay; SO/FG, safranin O-fast green; TEM, transmission electron microscopy.

https://doi.org/10.2147/JIR.S535311

MR Analysis

Data Sources

Summary statistics for the 60 cytokines and KOA were obtained from the IEU OpenGWAS database (https://gwas.mrcieu.ac.uk/). The most comprehensive genome-wide association study of cytokines was selected. Single-nucleotide polymorphisms (SNPs) associated with cytokines were obtained from the UK Biobank. The summary data for KOA was available from the European Bioinformatics Institute with the dataset number "ebi-a-GCST007090", which consisted of 403,124 samples (24,955 cases and 378,169 controls), and a total of 29,999,696 SNPs were genotyped. This large dataset provides a robust foundation for MR analysis, enabling a detailed examination of the potential causal pathways linking cytokines and KOA risk.

Selection of Genetic Instrumental Variables (IVs)

The fundamental aspect of MR studies is the use of SNPs as IVs, which are required to satisfy three critical assumptions:[29] (1) IVs are robustly associated with cytokines (association hypothesis); (2) IVs are independent of any confounders between cytokines and KOA (independence assumption); and (3) IVs affect KOA exclusively via their effects on cytokines rather than through any direct pathway (exclusivity hypothesis).

Several rigorous quality control steps were implemented to ensure the selection of optimal IVs. First, SNPs were chosen based on their strong relationship with the exposure ($P<1\times10^{-5}$) and lack of linkage disequilibrium ($r^2<0.001$ and clump window >10,000 kb). Second, the strength of the IVs was assessed using the F-statistic, with values >10 indicating a minimal risk of weak instrument bias.[30] Third, SNPs with a minor allele frequency of ≤0.01 were excluded.[31] Additionally, SNPs were harmonized between the exposure and outcome datasets, removing those with palindromic sequences and allelic inconsistencies (eg, C/T vs C/A).[32] The final set of SNPs was then used for MR analysis.

Statistical Analysis

This study utilized five distinct MR approaches to evaluate the causal relationship between cytokines and KOA. Each approach operated under different assumptions of horizontal pleiotropy. The primary method employed was the inverse variance-weighted (IVW) method. This standard MR technique combines Wald estimates from multiple genetic variants, which are calculated as the ratio of SNP–outcome associations to SNP–exposure associations.[33] These estimates are weighted by the inverse variance of the SNP–outcome associations, providing a powerful and precise approach to assess causal relationships. Furthermore, complementary analyses were performed using the weighted median, weighted mode, simple mode, and MR-Egger methods. These methods are particularly valuable because they can produce robust causal estimates even when some instrumental variables do not satisfy the ideal assumptions as long as the majority are valid. This adds an additional layer of reliability to the analysis, particularly for complex genetic data.[34,35]

All statistical analyses were two-sided, and a *P*-value of <0.05 was considered statistically significant. Statistical analysis and data visualization were conducted using R software (version 4.0.2), TwoSampleMR (version 0.5.6), and forestploter packages.

Sensitivity Analysis

Sensitivity analyses were conducted to ensure the robustness of the findings and to address any potential violations of the MR assumptions. First, horizontal pleiotropy was detected using the Egger intercept and MR-Pleiotropy Residual Sum and Outlier methods (MR-PRESSO) based on SNP levels and global heterogeneity estimates.[36] Cochran's Q test was used to assess the heterogeneity. Furthermore, a leave-one-out (LOO) analysis was performed to test the stability of these findings. Each SNP was discarded and the MR analysis was subsequently performed to assess whether the results were heavily influenced by a single SNP.[37] Finally, MR Steiger tests were conducted to verify the causal direction.

Vivo Experiment in Rats

Animals and Groups

A total of 36 male Sprague–Dawley rats (weight, 280–320 g; age, 8–9 weeks) obtained from Beijing Vital River Laboratory Animal Technology Co., Ltd. (SCxK [Jing] 2021–0006) were housed individually under controlled conditions (20±2 °C; 40–50% humidity) with 12-h light cycles and ad libitum access to standard chow and water.

All procedures were approved by the Animal Experimental Ethics Committee of Henan University of Chinese Medicine (IACUC-202309024). The instrument and reagent specifications are presented in Supplementary Table S1.

Following a 1-week acclimation period, the rats were randomly allocated to the blank control (BC) group (n=9) or model control (n=27) group using a random number table Post-modeling verification (1 rat/group), the remaining model rats were equally divided into three groups (n=8/group): model control (MC) group, Tuina therapy (TT) group, and positive drug (PD) group.

Establishment of a Rat Model of KOA

The KOA rat model was established through an intra-articular injection of papain using the following protocol:[38] activated papain solution was prepared by mixing 4% papain with 0.03 mol/L L-cysteine (2:1 ratio) in sterile saline, followed by activation for 30 min at room temperature. Twenty-seven fasted rats were anesthetized using an intraperitoneal injection of 3% sodium pentobarbital (3 mg/100 g). After right knee hair removal and iodophor disinfection, 0.2 mL of activated solution was injected into the joint cavity through the lateral patellar tendon under 45° knee flexion. This procedure was repeated weekly for three cycles (days 1, 4, and 7). After three injections, behavioral changes were assessed using the Lequesne MG rating scale. One rat from each group was randomly selected for hematoxylin and eosin staining, and the degree of knee cartilage degeneration was evaluated using the Mankin score. A Lequesne MG score of >4 and a Mankin score of ≥6 indicated a successful KOA model construction.[39]

Intervention Methods

Tuina group: The rats were immobilized on a fixation plate and the right knee treatment site was exposed. For details regarding Tuina intervention, please refer to our previous research methods.[40] In brief, the procedure is described as follows: (1) Acupressure manipulation: Four acupoints on the right hind limb of rats—Dubi (ST35), Yinlingquan (SP9), Yanglingquan (GB34) and Neixiyan (EX-LE4)—were stimulated using a specialized animal acupoint massaging instrument (Patent No. ZL201922406881.8) developed by our research group. Each acupoint received 2 minutes of pressure at a controlled intensity of 3–5 N and a standardized frequency of 60 compressions per minute. (2) Knee flexion and extension: A Finger TPS tactile pressure measurement system (PPS Inc., USA) was mounted on the operator's digits. The rat's knee joint was initially flexed, followed by the application of downward pressure to the inferior patellar border using the thumb, with concurrent knee extension under a stimulation force of 50 N. Repeat this 10 times.

The Tuina intervention was administered daily for 14 consecutive days by a single trained practitioner to ensure treatment consistency and minimize operator-related variability.

Positive drug group: Celecoxib was dissolved in normal saline, and a solution with a 2.4 mg/mL concentration was prepared. Rats in the celecoxib group were administered 10 mL/kg celecoxib solution once daily for 2 weeks.

Blank and model control groups: The blank and model groups were administered 1 mL/kg/d of normal saline continuously for 2 weeks.

Sampling

Following a 12-hour fast, rats were weighed, and the right knee region was shaved. Under anesthesia, the right knee joint was disinfected using standard aseptic techniques. Rats were then transferred to an ice-cooled platform with the right knee exposed. Articular cartilage specimens were harvested from the medial tibial plateau and medial femoral condyle of the right knee joint. These samples were preserved for subsequent analyses, including TEM, SO/FG staining, and cartilage-specific ELISA.

Behavioral Assessment

1. Lequesne MG: According to the evaluation criteria of the Lequesne MG rating scale, the behavioral performance of each rat was subdivided into four key dimensions: pain, joint motion, gait and joint swelling. Based on the above four dimensions, specific scores were assigned according to the Lequesne scale, and the scores for each item were recorded for a comprehensive evaluation.

2. Heat pain threshold (HPT): One week prior to testing, all rats underwent daily 30-min habituation sessions in plexiglass chambers to ensure environmental acclimatization. During the thermal nociception assessment, the rats were positioned on a preheated stainless-steel plate maintained at 50±0.5 °C using a digital thermoregulatory system. The latency to the first nocifensive response (defined as active hindpaw withdrawal with clear postural adjustment) was automatically recorded using integrated pressure sensors upon contact initiation. Each rat underwent three consecutive trials spaced by a minimum 40-min intertrial interval to prevent thermal sensitization, with final pain thresholds calculated as the mean response latency across valid trials. To ensure ethical compliance and prevent tissue injury, a predetermined safety cutoff of 35s was implemented, at which point the animals were immediately removed from the thermal surface and assigned a maximum latency value.
3. Gait analysis score (GAS): The rats in each group were made to exercise on an animal-powered treadmill for 20s (treadmill speed, 16 cm/s), and gait behavior was evaluated by 0–4 score semi-quantitative method.

Lequesne MG, HPT, and GAS scores were measured after modeling and 2 weeks of treatment.

SO/FG Staining

The knee tissue of rats was soaked in 4% paraformaldehyde for 24 h. After fixation, the sample was dehydrated with 10% ethylenediaminetetraacetic acid decalcified solution, impregnated with wax, sagittal embedding, and sliced into 3-μm sections. After the paraffin sections were dewaxed in water, they were stained with solid green and ferranine, and xylene was transparent. Cartilage morphology was systematically analyzed under an optical microscope at 200× magnification, and tissue area quantification was performed using ImageJ software by calculating the percentage of safranin O–positive cartilage matrix relative to the total articular surface area.

TEM

The tissue samples were subjected to standard electron microscopy processing as follows: After thorough cleaning, the specimens were fixed, rinsed, dehydrated, and embedded in resin, followed by oven polymerization. Ultrathin sections (thickness, 60–80 nm) were prepared using an ultramicrotome and mounted on 150-mesh copper grids. Grid-mounted sections were subjected to uranyl acetate staining under light-protected conditions, followed by rinsing and counterstaining with lead citrate in a carbon dioxide–free environment to prevent precipitate formation. Following a final rinse with ultrapure water and complete drying, the samples were examined using TEM. Quantitative analysis of autophagosomes was performed at 3000× magnification, whereas ultrastructural morphological evaluation was conducted at 8000× magnification.

Measurement of Autophagy-Related Cytokine Levels in the Articular Cartilage by ELISA

Autophagy-related cytokines in the cartilage that were causally related to KOA in MR Analysis were detected by ELISA. The procedure is described as follows: (1) Sample Pretreatment: Cartilage specimens were dissected into 1–3-mm^3 fragments and transferred to a pre-chilled mortar. Following the addition of ice-cold lysis buffer, tissues were homogenized under cryogenic conditions. The resultant homogenate was centrifuged at 4 °C (12,000× g for 15 min) to obtain the supernatant for subsequent analysis. (2) Test Procedure: Standard solutions were prepared by 1:1 dilution with the assay buffer. Both standard solutions and test samples were aliquoted into the designated wells of a microtiter plate, followed by the sequential addition of detection antibodies and assay buffer. After enzyme conjugate incubation and subsequent plate washing, the chromogenic substrate was added under light-protected conditions for development at room temperature. The enzymatic reaction was terminated using a stop solution, followed by the immediate measurement of optical density at 450 nm using a microplate reader. Final concentrations were calculated using standard curve interpolation.

Statistical Analysis

Statistical analyses were performed using SPSS (version 26.0; IBM Corp.) and GraphPad Prism 8.0 (GraphPad Software), with the latter used for graphical representation. Continuous variables are presented as means ± standard error of the mean. For multigroup comparisons, we conducted a one-way analysis of variance followed by post hoc analyses. The least significant difference method was applied for pairwise comparisons between groups, and Bonferroni correction was implemented to adjust for multiple comparisons. Statistical significance was set to $P < 0.05$ for all analyses.

ML Model

Data Sets and Preprocessing

We selected 12 intraexperimental indicators as input features for the ML model. These variables included behavioral assessments (Lequesne MG, HPT, and GAS), staining measures (percentage cartilage area), TEM detection (relative autophagy level), and measurement of autophagy-related cytokine levels (interferon gamma [IFN-γ], IL-1β, parathyroid hormone [PTH], IL-17, MMP-3, osteocalcin [OCN], and TGF-β1). Text labels in the in-vivo experimental data were converted into digital labels using one-hot encoding, and the dataset was normalized. The selected features were then analyzed to simplify the number of features and remove inappropriate features, thereby improving the stability and robustness of model training.

Model Construction

In Python 3.12.3, an SVM model was implemented using the Sklearn.svm tool. This model operates based on the principles of the maximum margin classification and kernel methods.[41] The SVM algorithm identifies an optimal hyperplane in the feature space to separate the data points of different classes. This hyperplane is determined by support vectors, which are the data points closest to the decision boundary, with the margin representing the distance between the hyperplane and the nearest instances. The objective of the model is to maximize the margin to achieve optimal class separation.

The algorithm employs kernel functions (including linear, polynomial, and radial basis function [RBF] kernels) to transform data from the original feature space into higher-dimensional representations, facilitating the identification of separable hyperplanes. The selection of the kernel type and associated parameters (such as the polynomial degree or RBF gamma value) significantly influences model performance.[42] Optimization involves solving a quadratic programming problem that simultaneously maximizes the margin and minimizes the number of classification errors. Hyperparameter tuning through grid search and cross-validation ensures the optimal configuration of critical parameters (eg, regularization parameter C and kernel parameters). After determining the optimal hyperparameters, the final SVM model was trained on the complete dataset, thereby enabling the classification of new and unseen data points. Its performance on the test set was directly used to evaluate the correlation between different evaluation measures and predict the overall and categorical efficacy of treatment measures.[43]

Model Evaluation

Initially, the performance of the SVM model was evaluated using three key metrics: accuracy, F1 score, and Cohen's kappa coefficient. Accuracy quantifies the proportion of correctly classified samples relative to the total test set and serves as a fundamental measure in classification tasks.[44] The F1 score (harmonic mean of precision and recall) and kappa coefficient (inter-rater agreement measurement) provide complementary assessments of classification consistency with the ground truth. A comprehensive performance analysis was conducted using a confusion matrix, where rows represent actual classes and columns indicate predicted classifications, with matrix cells containing sample counts for each actual–predicted class combination.[45] To enhance interpretability, we implemented matrix normalization and generated visual heatmap representations.

Following the validation of the effectiveness of the SVM model, we leveraged its optimal hyperplane separation principle to conduct goodness-of-fit tests on 12 standardized indicator sets and their combinations. The R-squared (R^2) metric was employed to quantitatively evaluate the correlation strength between the individual indicators and their combined effects.[46]

Finally, we selected the data of the blank control and model groups as the training and testing sets, respectively. Subsequent predictions were made for pharmacological and Tuina therapy interventions to assess their therapeutic efficacy. Two levels of efficacy evaluation were conducted for each indicator: overall efficacy analysis of Tuina on KOA, and comprehensive effects analysis of the index type (behavioral characteristics, cartilage degeneration features, and autophagy-related cytokines).

Results

Selection of Genetic IVs

After filtering for strong correlations ($P<1\times10^{-5}$) and ensuring independence ($r^2<0.001$), significant and independent SNPs were included in the analysis. This process resulted in the selection of 1544 SNPs as IVs for 60 cytokines. Each SNP related to cytokines had an F-statistic of >10, suggesting a low risk of weak instrumental bias influencing the results.

The Causal Relationship Between Cytokines and KOA

MR analysis revealed significant causal associations between 8 of 60 cytokines and KOA, with genetic evidence supporting either positive or negative effect estimates for these identified biomarkers. The IVW estimations demonstrated that higher genetically predicted levels of IFN-γ (odds ratio [OR], 1.02; 95% confidence interval [CI], 1.00–1.04; *P*=0.046), IL-17 (OR, 1.05; 95% CI, 1.01–1.09; *P*=0.013), PTH (OR, 1.03; 95% CI, 1.00–1.06; *P*=0.041), and IL-1β (OR, 1.02; 95% CI, 1.00–1.04; *P*=0.026) were related to a higher KOA risk. Conversely, an increased genetic predisposition toward TGF-β1 (OR, 0.85; 95% CI, 0.77–0.99; *P*=0.048), MMP-3 (OR, 0.96; 95% CI, 0.93–0.99; *P*=0.021), MMP-10 (OR, 0.96; 95% CI, 0.93–0.99; *P*=0.022), and OCN (OR, 0.88; 95% CI, 0.78–0.99; *P*=0.041) were associated with a lower KOA risk. The robustness of the MR effect estimates was confirmed using complementary methods. Importantly, MR analysis conducted in the reverse direction did not provide any reliable evidence to suggest that KOA may be the cause of changes in cytokine levels.

After a comprehensive analysis of the cytokines causally associated with KOA, we found that, except for MMP-10, the other seven cytokines regulated or participated in the chondrocyte autophagy process, indicating that autophagy plays an important role in the occurrence and development of KOA. Figure 2 shows the summary results of the MR analysis, and Figure 3 illustrates a forest plot of the eight causal relationships identified by the MR Analysis.

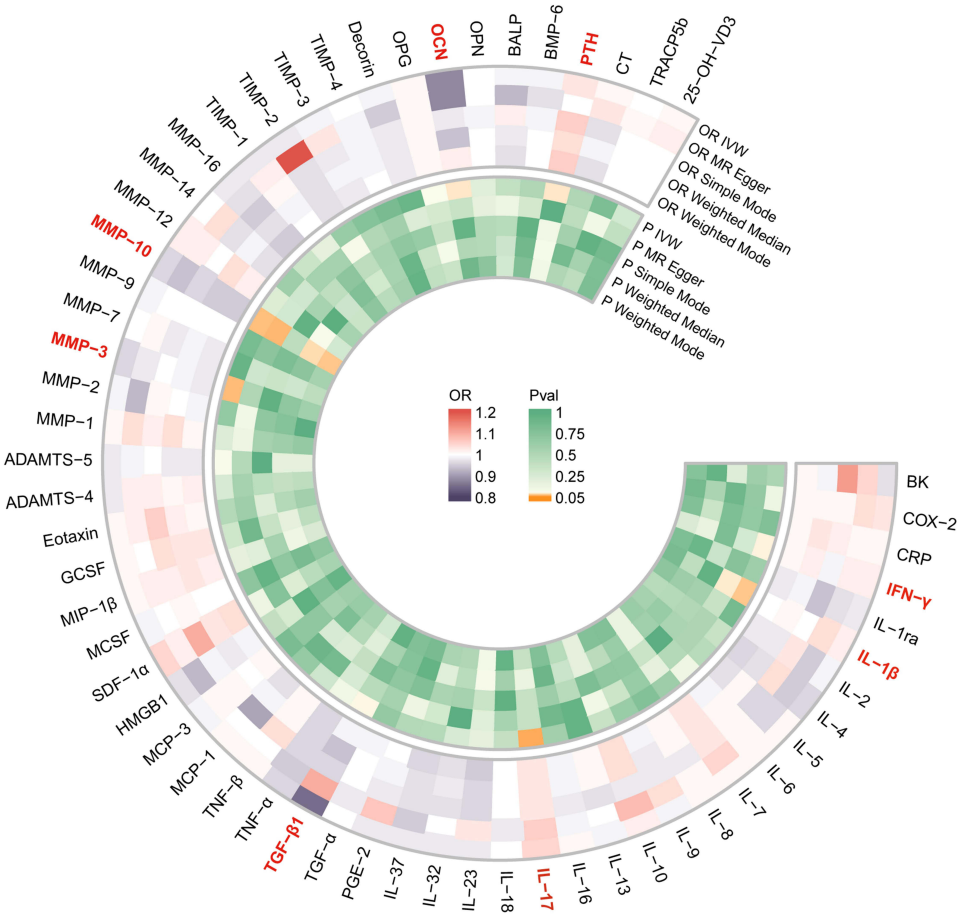

Figure 2 The summary results of the MR Analysis.
Note: The bold red text indicates that the P value is less than 0.05, which is statistically significant.
Abbreviations: BK, bradykinin; COX-2, cyclooxygenase-2; CRP, C-reactive protein; IFN-γ, interferon-γ; IL-1ra, interleukin-1 receptor antagonist; IL-1β, interleukin-1 beta; PGE-2, prostaglandin E2; TGF-α, transforming growth factor-alpha; TGF-β1, transforming growth factor-beta 1; TNF-α; tumor necrosis factor-alpha; TNF-β, tumor necrosis factor-beta; MCP-1, monocyte chemotactic protein-1; HMGB1, high mobility group box 1; SDF-1α, stromal cell-derived factor 1 alpha; MCSF, macrophage colony-stimulating factor; MIP-1β, macrophage inflammatory protein 1 beta; GCSF, granulocyte colony-stimulating factor; ADAMTS-4, a disintegrin and metalloproteinase with thrombospondin 4; MMP-1, matrix metalloproteinase-1; TIMP-1, tissue inhibitor of metalloproteinases-1; OPG, osteoprotegerin; OCN, osteocalcin; OPN, osteopontin; BALP, bone alkaline phosphatase; BMP-6, bone morphogenetic protein-6; PTH, parathyroid hormone; CT, calcitonin; TRACP5b, tartrate-resistant acid phosphatase type 5b; 25-OH-VD3, 25-hydroxyvitamin D3.

Exposure	Outcome	Methods	nSNP	Beta	SE	Pval	OR(95%CI)
IFN-γ	KOA	Inverse Variance Weighted	31	0.0223	0.0112	**0.046**	1.02(1.00-1.04)
		MR Egger	31	0.0212	0.0192	0.278	1.02(0.98-1.06)
		Weighted Median	31	0.0224	0.0159	0.157	1.02(0.99-1.05)
		Simple Mode	31	-0.0085	0.0363	0.815	0.99(0.92-1.06)
		Weighted Mode	31	0.0190	0.0161	0.249	1.01(0.98-1.05)
IL-1β	KOA	Inverse Variance Weighted	14	0.0238	0.0107	**0.026**	1.02(1.00-1.04)
		MR Egger	14	0.0472	0.0209	**0.043**	1.04(1.01-1.09)
		Weighted Median	14	0.0123	0.0150	0.411	1.01(0.98-1.04)
		Simple Mode	14	0.0013	0.0248	0.956	1.00(0.95-1.05)
		Weighted Mode	14	0.0050	0.0231	0.829	1.00(0.96-1.05)
IL-17	KOA	Inverse Variance Weighted	5	0.0491	0.0198	**0.013**	1.05(1.01-1.09)
		MR Egger	5	0.1560	0.0501	0.374	1.06(0.97-1.16)
		Weighted Median	5	0.0370	0.0251	0.141	1.03(0.98-1.09)
		Simple Mode	5	0.0341	0.0342	0.375	1.03(0.96-1.10)
		Weighted Mode	5	0.0331	0.0335	0.378	1.03(0.96-1.10)
TGF-β1	KOA	Inverse Variance Weighted	9	-0.1510	0.0768	**0.048**	0.85(0.73-0.99)
		MR Egger	9	0.1320	0.1667	0.452	1.10(0.92-1.28)
		Weighted Median	9	-0.0550	0.0973	0.569	0.94(0.78-1.13)
		Simple Mode	9	-0.0380	0.1552	0.811	0.96(0.71-1.29)
		Weighted Mode	9	-0.0061	0.1177	0.959	0.99(0.78-1.25)
MMP-3	KOA	Inverse Variance Weighted	50	-0.0360	0.0150	**0.021**	0.96(0.93-0.99)
		MR Egger	50	-0.0160	0.0250	0.509	0.98(0.93-1.03)
		Weighted Median	50	-0.0080	0.0220	0.705	0.99(0.94-1.03)
		Simple Mode	50	0.0010	0.0490	0.971	1.00(0.90-1.10)
		Weighted Mode	50	-0.0110	0.0210	0.600	0.98(0.94-1.03)
MMP-10	KOA	Inverse Variance Weighted	44	-0.0330	0.0140	**0.022**	0.96(0.93-0.99)
		MR Egger	44	-0.0540	0.0220	**0.019**	0.94(0.90-0.98)
		Weighted Median	44	-0.0440	0.0210	**0.036**	0.95(0.91-0.99)
		Simple Mode	44	-0.0330	0.0400	0.417	0.96(0.89-1.04)
		Weighted Mode	44	-0.0450	0.0190	**0.026**	0.95(0.91-0.99)
OCN	KOA	Inverse Variance Weighted	26	-0.1218	0.0597	**0.041**	0.88(0.78-0.99)
		MR Egger	26	-0.1540	0.1673	0.365	0.88(0.71-1.05)
		Weighted Median	26	0.0588	0.0841	0.492	0.94(0.79-1.11)
		Simple Mode	26	-0.0121	0.1704	0.938	0.98(0.75-1.21)
		Weighted Mode	26	0.0227	0.1578	0.884	1.02(0.80-1.24)
PTH	KOA	Inverse Variance Weighted	26	0.0301	0.0148	**0.041**	1.03(1.00-1.06)
		MR Egger	26	0.0007	0.0378	0.983	1.00(0.92-1.07)
		Weighted Median	26	0.0398	0.0218	0.068	1.04(0.99-1.08)
		Simple Mode	26	0.0659	0.0390	0.103	1.06(0.98-1.15)
		Weighted Mode	26	0.0617	0.0351	0.091	1.06(0.98-1.14)

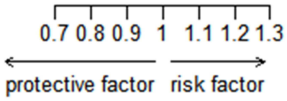

Figure 3 The forest plot of the eight causal relationships identified by the MR Analysis.
Note: The bold red text indicates that the P value is less than 0.05, which is statistically significant.
Abbreviations: IFN-γ, interferon-γ; IL-1β, interleukin-1 beta; IL-17, interleukin-17; TGF-β1, transforming growth factor-beta 1; MMP-3, matrix metalloproteinase-3; MMP-10, matrix metalloproteinase-10; OCN, osteocalcin; PTH, parathyroid hormone; KOA, knee osteoarthritis; SE, standard error; OR, odds ratio; CI, confidence interval.

https://doi.org/10.2147/JIR.S535311

The Cochran's Q test indicated no evidence of heterogeneity, whereas both the MR-Egger intercept and MR-PRESSO global tests revealed no indication of directional pleiotropy bias. Moreover, LOO analysis did not detect any SNP outliers, further validating the consistency and durability of the MR analysis. The results of the sensitivity analysis are presented in Supplementary Table S2 and Supplementary Figures S1-8.

Effects of Tuina on the Lequesne MG, HPT and GAS in KOA Rats

Lequesne MG, HPT, and GAS were performed to systematically evaluate the therapeutic effects of Tuina on KOA in rats. As shown in Figure 4A–C, all experimental groups exhibited significant differences compared with the blank control group in post-modeling assessments ($P<0.05$), confirming the successful establishment of the KOA rat model. Post-intervention analysis revealed that both the Tuina therapy and positive control (celecoxib) groups demonstrated marked improvements in Lequesne MG, HPT, and GAS compared with the model group (Figure 4D–F, $P<0.05$). Notably, although Tuina showed comparable efficacy to celecoxib in normalizing HPT responses ($P>0.05$), it exhibited superior therapeutic effects in reducing Lequesne MG and enhancing GAS compared with the positive drug group ($P<0.05$).

Histopathological Changes in the Articular Cartilage

As illustrated in Figure 5A, SO/FG staining showed that the blank group exhibited a well-preserved articular cartilage architecture, characterized by an intact superficial layer, continuous surface regularity, and physiological cartilage thickness with normal cellular distribution. By contrast, the model group showed marked pathological alterations, including extensive superficial cartilage erosion, substantial depletion of extracellular matrix components, significant chondrocyte depletion, and decreased cartilage thickness. Compared with the model group, the thickness of the articular cartilage in the Tuina group increased, the number of chondrocytes increased, and the surface wear of the cartilage

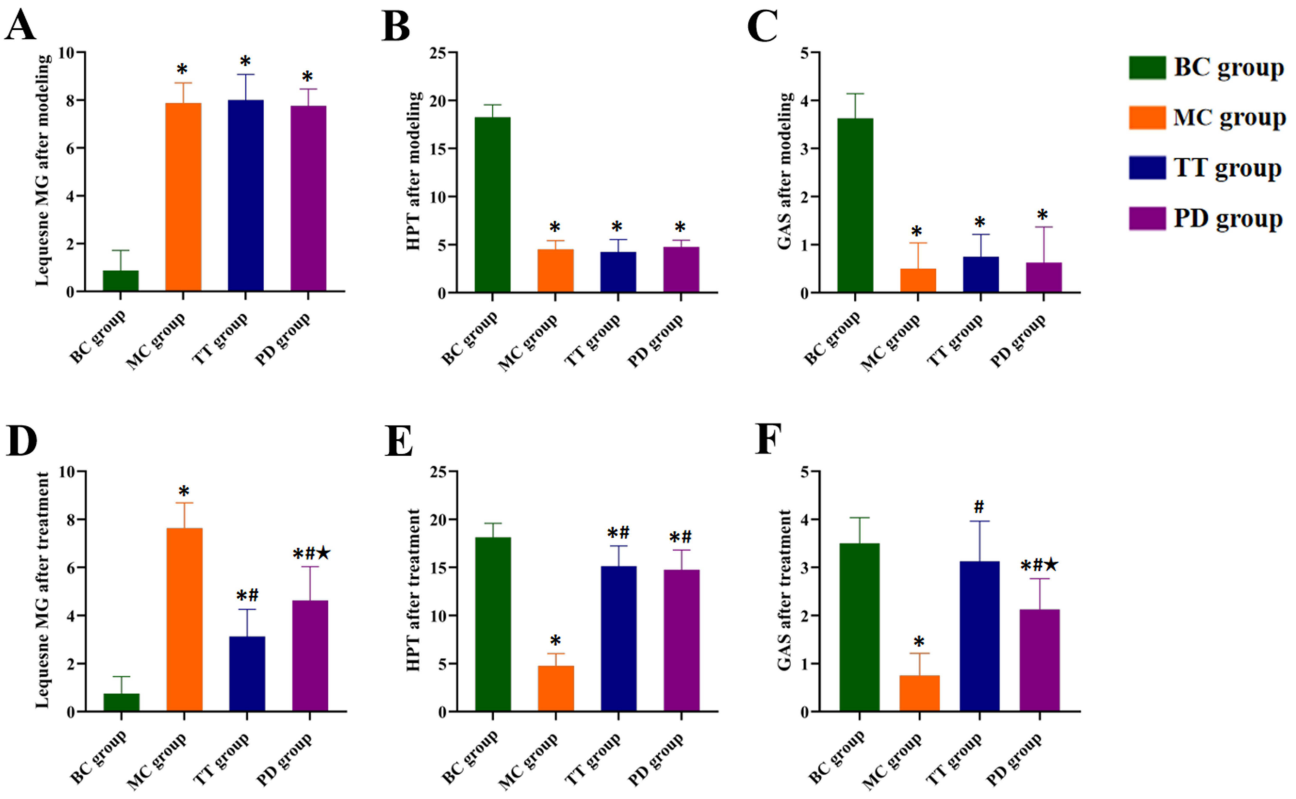

Figure 4 Effect of Tuina on behavioral indicators of the knee joint in KOA rats.
Notes: (**A–C**), Lequesne MG, HPT and GAS after modeling of KOA rats in each group; (**D–F**), Lequesne MG, HPT and GAS after treatment. *Compared with blank control group, $P<0.05$; #Compared with model control group, $P<0.05$; ★Compared with Tuina therapy group, $P<0.05$.
Abbreviations: BC, blank control; MC, model control; TT, Tuina therapy; PD, positive drug.

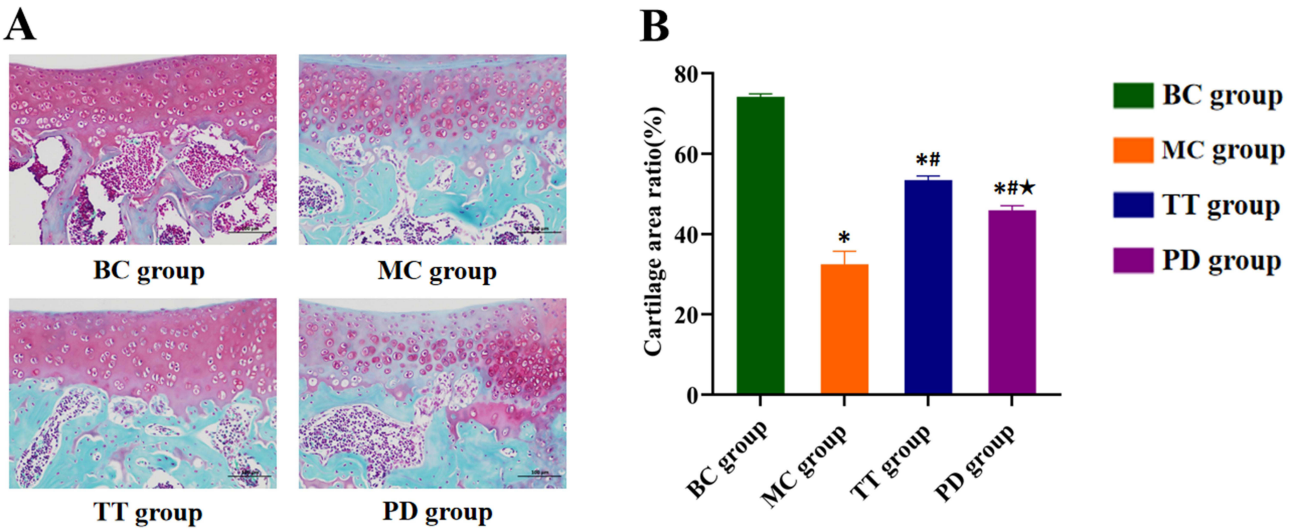

Figure 5 (**A**) Observation results of SO/FG stained knee cartilage of rats in each group under light microscope. Scale, 200μm. (**B**) Cartilage area ratio in each group.
Note: *Compared with blank control group, $P<0.05$; # Compared with model control group, $P<0.05$; ★ Compared with Tuina therapy group, $P<0.05$.
Abbreviations: BC, blank control; MC, model control; TT, Tuina therapy; PD, positive drug.

decreased. In the positive drug group, the chondrocytes of the articular cartilage and their thickness slightly increased; however, the articular cartilage was not smooth, and the chondrocytes were partially deformed.

To observe the changes in the cartilage tissue in each group more accurately, the percentage of the cartilage area was quantitatively assessed. As shown in Figure 5B, the percentage of the cartilage area in the Tuina and positive-drug groups was significantly higher than that in the model group ($P<0.05$). In addition, the percentage of the cartilage area in the Tuina group was higher than that in the positive-drug group ($P<0.05$), demonstrating the superior therapeutic efficacy of Tuina in cartilage repair in KOA rat models.

TEM Assessment

Figure 6A shows the ultramorphological changes in articular chondrocytes in each group at 8000× magnification. In the blank group, chondrocytes exhibited intact cellular membranes, a dense perinuclear cartilage matrix, and well-preserved organelles (including nuclei with a regular morphology, abundant mitochondria with intact membranes, and rough endoplasmic reticulum [RER] densely studded with ribosomes). Autophagosomes and lysosomes were present at physiological levels. Conversely, the model group displayed marked degeneration, including chondrocyte shrinkage, matrix dissolution with delicate fibrillar networks, organelle swelling, nuclear membrane invagination, mitochondrial depletion (membrane disruption and cristae fragmentation), and dilated RER. Notably, the number of autophagosomes and autophagolysosomes was abnormally increased.

Compared with the model group, the Tuina group showed significant recovery of the cell structure: intact membranes with short cytoplasmic projections, regular nuclei with condensed chromatin, restored mitochondrial integrity (reduced cristae fragmentation and matrix dilution), and a normalized RER structure with ribosome reattachment. Autophagic vacuoles decreased to near-normal levels, and the positive-drug group demonstrated partial improvement, including reduced RER dilation and a moderate autophagosome decrease. However, persistent pathological features, including cytoplasmic contractions, swollen organelles, mitochondrial membrane dissolution, partial cristae disruption, and nuclear atrophy with indistinct membranes, were observed.

To evaluate the autophagy of chondrocytes in each group, the relative number of autophagosomes was quantitatively analyzed using TEM at 3000× magnification. As shown in Figure 6B and C, the model group exhibited a significant increase in the number of relative autophagosomes compared with that in the blank control group ($P<0.05$). Notably, both the Tuina therapy and positive drug intervention effectively reduced the relative autophagy levels compared with those in

https://doi.org/10.2147/JIR.S535311

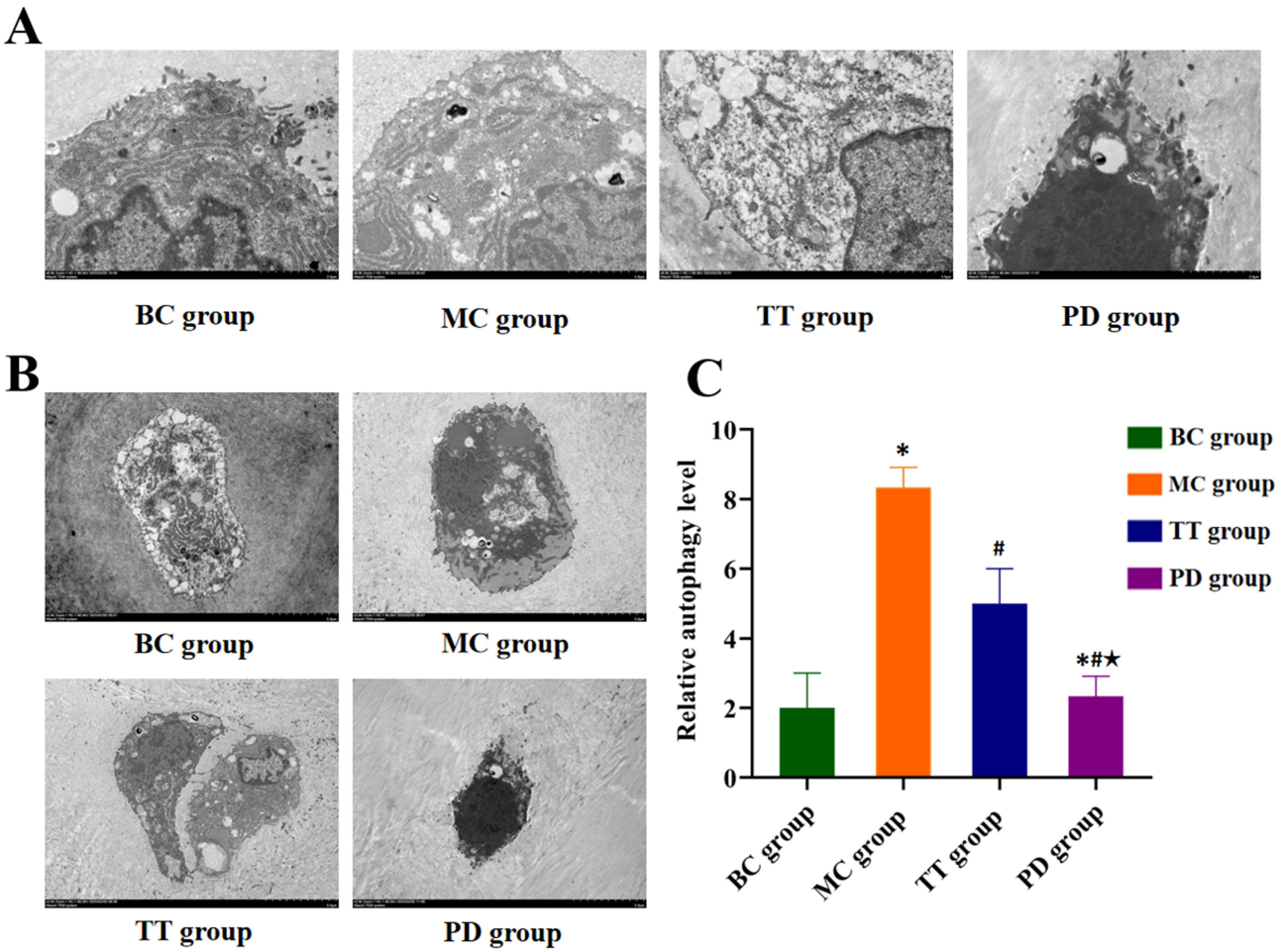

Figure 6 Observation results of knee cartilage of rats in each group under under 8000x (**A**) and 3000x (**B**) TEM. (**C**) relative autophagy level in each group.
Notes: *Compared with blank control group, *P*<0.05; # Compared with model control group, *P*<0.05; ★ Compared with Tuina therapy group, *P*<0.05.
Abbreviations: BC, blank control; MC, model control; TT, Tuina therapy; PD, positive drug.

the model group ($P<0.05$). Importantly, the Tuina group demonstrated superior autophagy suppression compared with the positive drug group ($P<0.05$), indicating that Tuina has a better regulatory effect on chondrocyte autophagy homeostasis.

Effects of Tuina on Autophagy-Related Cytokines in Articular Cartilage of KOA Rats

ELISA results for autophagy-related cytokines in the rat knee cartilage are shown in Figure 7. The OCN and TGF-β1 levels were significantly decreased ($P<0.05$) and IFN-γ, IL-1β, PTH, IL-17, and MMP-3 levels were significantly increased in the model control group compared with those in the blank group ($P<0.05$). All treatment groups showed a reversal of these trends relative to the model group. Notably, although Tuina showed comparable efficacy to celecoxib in modulating IL-1β and IL-17 levels ($P>0.05$), it exhibited superior therapeutic effects in reducing IFN-γ, PTH, and MMP-3 levels and enhancing OCN and TGF-β1 expressions compared with celecoxib ($P<0.05$).

Performance of the SVM Model

The ML results indicated an accuracy of 91.67% for the SVM model, which remained stable in both univariate and multivariate analyses. The classification accuracy was supplemented by the F1 score and kappa coefficient. For each label of the four categories, the F1 scores were 1.00, 1.00, 0.75, and 1.00, respectively, with an overall kappa coefficient of 0.909. The resulting confusion matrix also confirmed the performance of the SVM model (Figure 8).

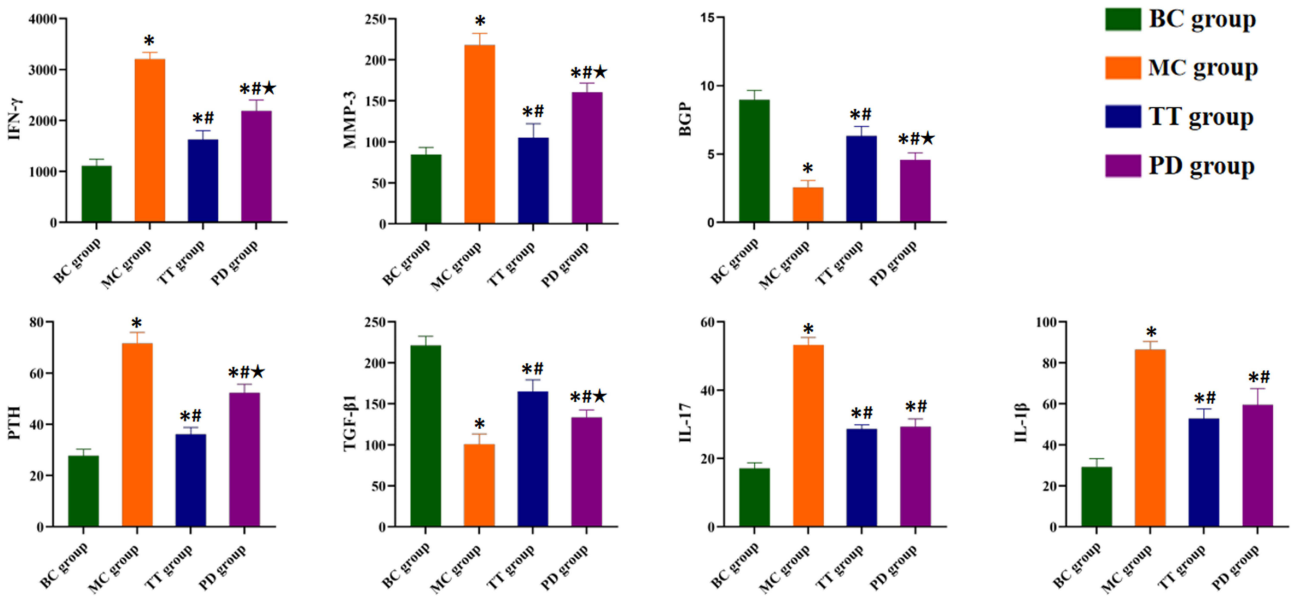

Figure 7 Effects of Tuina on the Levels of Autophagy-related Cytokines in Knee Cartilage Tissues of KOA Rats.
Note: *Compared with blank control group, $P<0.05$; # Compared with model control group, $P<0.05$; ★Compared with Tuina therapy group, $P<0.05$.
Abbreviations: BC, blank control; MC, model control; TT, Tuina therapy; PD, positive drug.

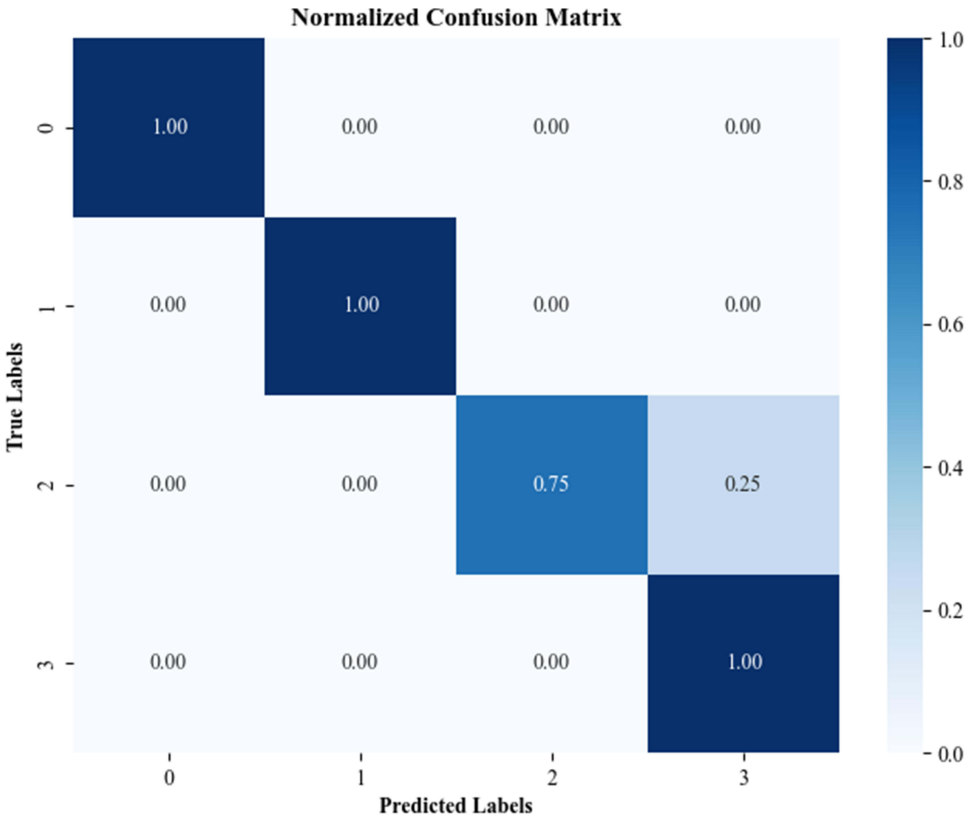

Figure 8 Confusion matrix diagram for model performance.
Note: The darker the color (from white to blue) of the squares in the matrix, the higher the weight of the edges.

https://doi.org/10.2147/JIR.S535311

Feature Correlation Analysis

The SVM model revealed both individual and categorical correlations among the input features (Figures 9 and 10). As presented in Figure 9, individual correlation analysis demonstrated that the highest-ranked associations predominantly involved autophagy-related cytokines. The strongest correlation was observed between IFN-γ and PTH (0.97), followed by TGF-β1 and OCN (0.93), and a negative correlation between IFN-γ and TGF-β1 (−0.92). Except for MMP-3, IL-1β, and IL-17, all other autophagy-related cytokines exhibited robust correlations with cartilage area ratio (CAR) and relative autophagy level (RAL). Notably, Lequesne MG also showed a strong association with CAR (0.90). As Figure 10 indicates, Categorical correlation analysis revealed that cartilage degeneration had the strongest association with autophagy-related cytokines (0.80) and the weakest association with behavioral assessments (0.24). In addition, there is also a strong correlation between autophagy level and cartilage degeneration (0.72).

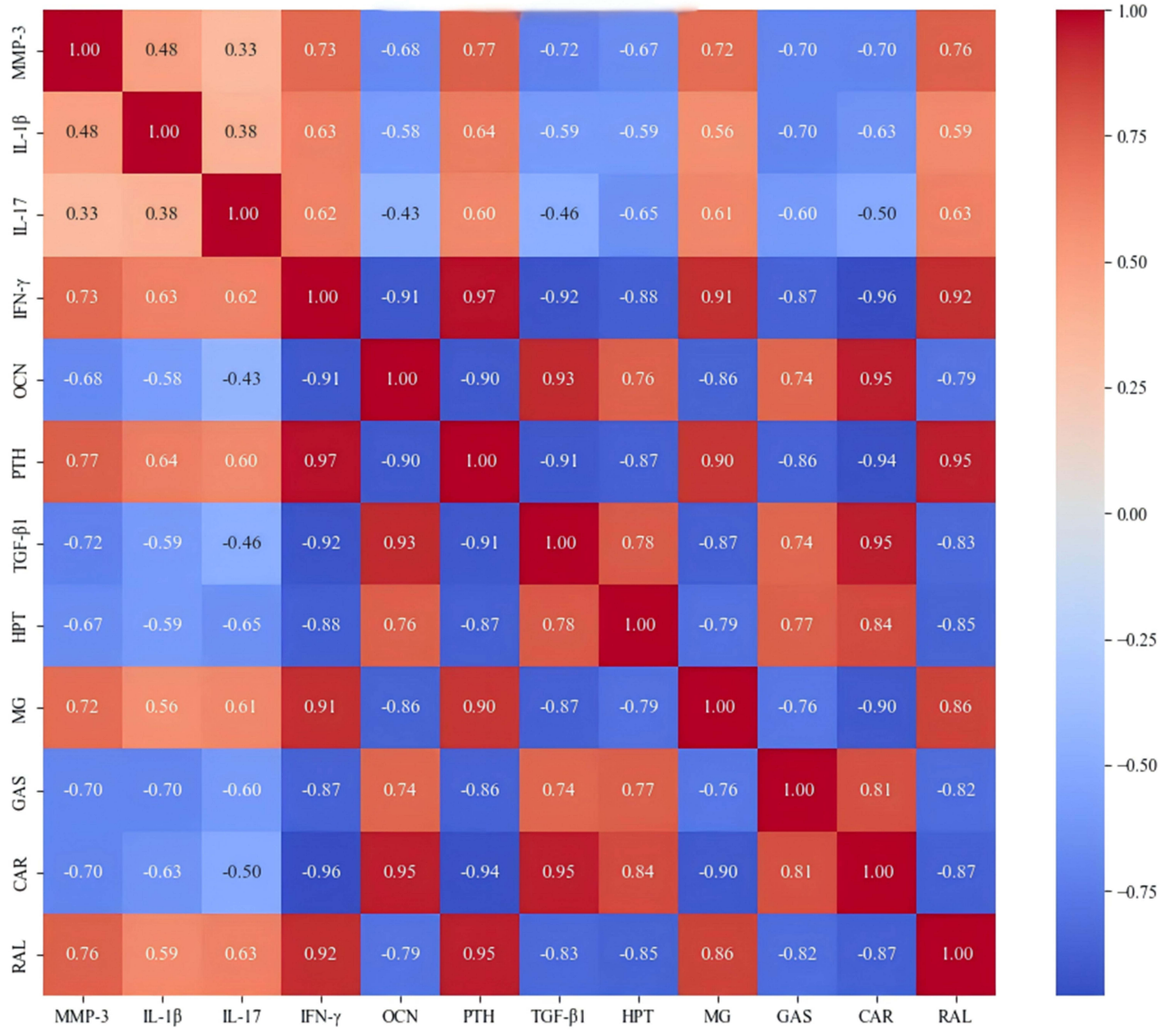

Figure 9 Individual correlation analysis in the SVM model.

Abbreviations: MMP-3, matrix metalloproteinase-3; IL-1β, interleukin-1 beta; IL-17, interleukin-17; IFN-γ, interferon-γ; OCN, osteocalcin; PTH, parathyroid hormone; TGF-β1, transforming growth factor-beta 1; HPT, heat pain threshold; MG, Lequesne MG; GAS, gait analysis score; CAR, cartilage area ratio; RAL, relative autophagy level.

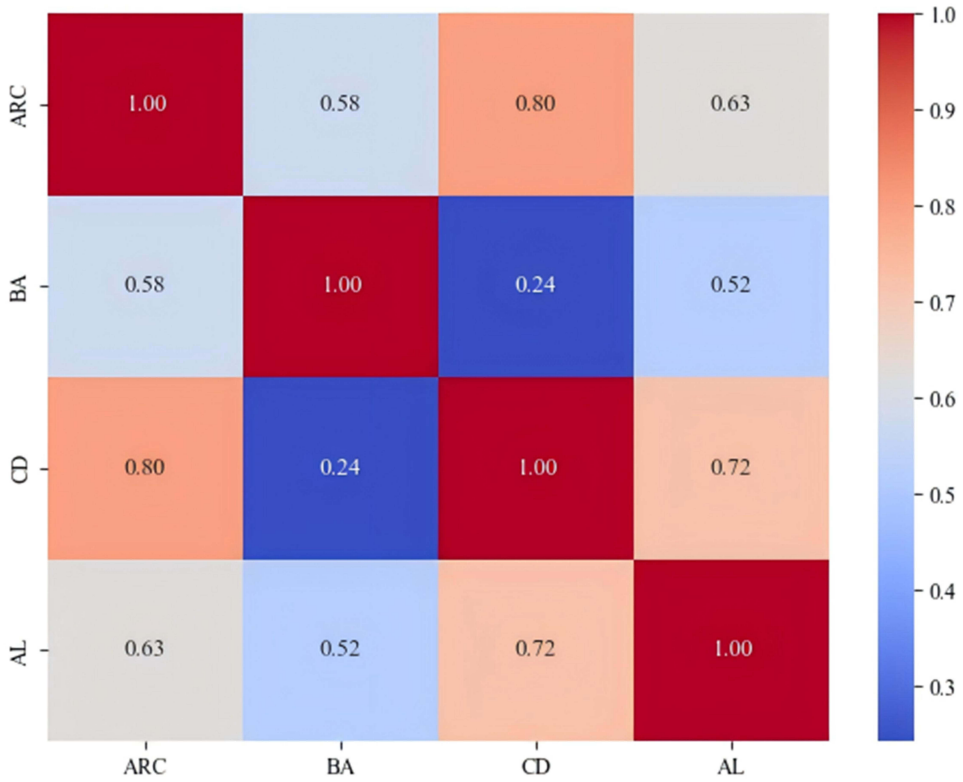

Figure 10 Categorical correlation analysis in the SVM model.
Abbreviations: ARC, autophagy-related cytokines; BA, behavioral assessment; CD, cartilage degeneration; AL, autophagy level.

Comprehensive and Classified Curative Effect Analyses

A confusion matrix was drawn to visually judge the effect of Tuina and celecoxib on KOA. As shown in Figure 11A, the comprehensive analyses of all included features revealed that the overall effect of Tuina on KOA was superior to that of

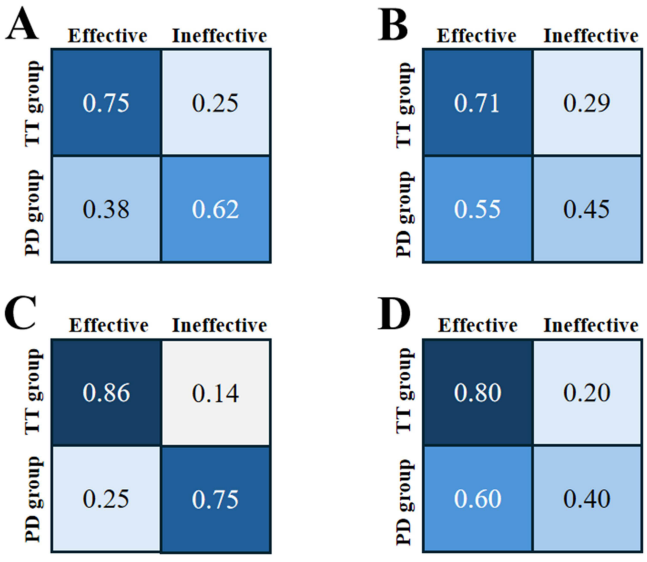

Figure 11 Confusion matrix diagram for curative effect analysis.
Notes: (**A**) overall effect; (**B**) behavioral characteristics; (**C**) cartilage degeneration-related metrics; (**D**) autophagy-related cytokines.
Abbreviations: TT, Tuina therapy; PD, positive drug.

https://doi.org/10.2147/JIR.S535311

celecoxib. In addition, feature indicators were classified and analyzed into three categories: behavioral characteristics, cartilage degeneration features, and autophagy-related cytokines. As shown in Figure 11B–D, the capacity of Tuina to improve behavioral metrics, cartilage degeneration, and autophagy-related cytokines was superior to that of celecoxib.

Discussion

KOA is a degenerative joint disorder characterized by cartilage degradation, driven primarily by dysregulated chondrocyte autophagy.[47,48] Following the onset of KOA, abnormalities in autophagy disrupt chondrocyte synthesis and metabolism, limiting the secretion of the extracellular matrix crucial for cartilage function and, ultimately, accelerating cartilage destruction. Emerging research has highlighted the pivotal role of cytokine-mediated modulation of autophagy in disrupting chondrocyte homeostasis and accelerating disease progression.[49] Specifically, IL-1β suppresses autophagy initiation by downregulating key regulators such as the ULK1 complex and Beclin-1, thereby promoting the accumulation of damaged mitochondria and misfolded proteins within chondrocytes.[50] This impairment exacerbates cellular degeneration and establishes a pathological feedback loop through MMP-3 overactivation, which amplifies extracellular matrix degradation and perpetuates cartilage destruction. Notably, IFN-γ contributes to this cascade by polarizing macrophages toward the pro-inflammatory M1 phenotype, which enhances IL-1β and TNF-α secretion.[51] Concurrently, IFN-γ disrupts the ATG5/ATG12 ubiquitination system, impairing autophagosome formation and intensifying oxidative stress in chondrocytes.[52] These synergistic mechanisms collectively compromise the cellular repair capacity and accelerate osteoarthritic degeneration. Although some studies have shown that Tuina therapy may slow the progression of KOA by regulating autophagy-related cytokine levels (eg, PTH, MMP-13, TGF-β1), it still has disadvantages such as being susceptible to confounding factors, unclear molecular targets, and single evaluation methods, and the conclusions need to be further systematically clarified.[53,54] To address the shortcomings of the aforementioned studies, we adopted a multidimensional approach combining MR, in vivo experiments, and ML to systematically reveal the mechanism of autophagy regulation by Tuina in the treatment of KOA.

MR analysis has emerged as an invaluable tool for identifying genetically regulated biomarkers associated with disease pathogenesis, effectively reducing the confounding biases inherent in experimental studies.[55] Our analysis, which incorporated eight distinct cytokines, revealed complex associations with the risk of KOA. Notably, we identified significant positive correlations between KOA susceptibility and four cytokines: IFN-γ, IL-1β, IL-17, and PTH. These findings suggest that elevated circulating levels of these cytokines may increase disease susceptibility, potentially through their involvement in autophagy-related pathways implicated in KOA pathogenesis. Conversely, our study revealed a negative correlation between KOA and MMP-3, MMP-10, TGF-β1, and OCN. This finding is particularly intriguing because it suggests that higher levels of these cytokines may confer protection against KOA. Notably, seven of the eight cytokines (except MMP-10) were functionally associated with chondrocyte autophagy regulation. Through a systematic evaluation of these genetic associations, we identified autophagy regulation as a key biological mechanism for the onset and progression of KOA, which provides a direction for subsequent mechanistic studies and high-confidence target prediction for therapeutic strategies for KOA.

To investigate the mechanism of action of Tuina in KOA, we established a rat KOA model using L-cysteine–activated papain injections. This model, which utilized papain to decompose proteoglycans in the cartilage matrix, mimics the early human KOA changes.[56,57] This modeling method has characteristics similar to those of human KOA and is a better method for studying KOA. This study investigated a therapeutic Tuina protocol comprising pressure application at acupoints and passive knee joint mobilization. The acupressure technique focused on two paired acupoint combinations from the Yin-Yang point pairing methodology: Dubì (ST35)–Neixiyan (EX-LE4) and Yinlíngquán (SP9)–Yánglíngquán (GB34). These complementary pairings from opposing meridians embody the TCM principle of "Yin-Yang harmonization", demonstrating synergistic therapeutic effects in KOA management through dynamic balance regulation. Precision pressure application at these acupoints facilitates multiple therapeutic actions, including promoting qi blood circulation, releasing soft tissue adhesions, enhancing microcirculation, and improving knee joint stability and mobility.[58,59] Concurrently, controlled passive mobilization of the knee joint induces biomechanical adjustments, effectively expanding articular space dimensions and redistributing intra-articular stress concentrations.[60] This dual-modality approach achieves the classical TCM objective of restoring proper bone alignment and soft tissue flexibility.

Autophagy-related cytokines in the cartilage that were causally related to KOA in the MR analysis were detected by ELISA. The results revealed elevated levels of IFN-γ, IL-1β, IL-17, PTH, and MMP-3 and decreased TGF-β1 and OCN levels in the cartilage of rat models. Tuina and celecoxib interventions reversed these changes, with Tuina showing superior efficacy in regulating IFN-γ, PTH, MMP-3, TGF-β1, and OCN than celecoxib. Notably, six of the seven cytokines, except MMP-3, followed the MR-predicted trends. TEM demonstrated excessive autophagosomes/autophagolysosomes and cellular degeneration in rat chondrocytes, whereas both interventions reduced autophagic activity. Tuina exhibited better morphological restoration and autophagy inhibition than the drug group. This study suggests that tuina ameliorates KOA by modulating autophagy-related cytokine networks and suppressing pathological chondrocyte autophagy.

Cartilage degeneration is the most significant pathological condition associated with KOA.[61,62] SO/FG staining demonstrated progressive cartilage degradation across all experimental groups except for the blank group, with the most severe manifestations observed in the model group. This group exhibited extensive articular surface erosion accompanied by the substantial depletion of extracellular matrix components and marked chondrocyte depletion. Pharmacological intervention with celecoxib showed moderate therapeutic effects, including the partial restoration of cartilage surface integrity, slight chondrocyte proliferation, and heterogeneous matrix recovery with minimal thickness improvement. By contrast, Tuina demonstrated superior cartilage preservation, presenting near-intact articular surfaces, enhanced cellularity with a relatively even distribution, and significantly increased cartilage thickness despite mild matrix disorganization. Quantitative morphometric analysis confirmed these observations, with both interventions showing significantly greater cartilage area percentages than that observed in model controls, whereas tuina outperformed celecoxib in this parameter. Behavioral assessments using Lequesne MG, HPT, and GAS revealed differential therapeutic efficacies. Both interventions significantly improved all three parameters compared with those observed in model controls. In addition to achieving equivalent analgesic effects in HPT restoration, Tuina demonstrated superior efficacy in Lequesne MG reduction and GAS enhancement, indicating enhanced antiedematous effects and functional recovery compared with pharmacological treatment. Mechanistically, our findings suggest that the therapeutic benefits of Tuina in KOA may involve the modulation of chondrocyte autophagy through cytokine-mediated regulation. This proposed mechanism aligns with the observed cartilage preservation outcomes, potentially offering a multitargeted approach to decelerate degenerative processes in osteoarthritic joints.

Given the limited predictive accuracy observed in animal experiments, we employed an SVM model to validate and complement these findings. The SVM model demonstrated robust performance, confirming the feasibility and rationality of the indicators selected for animal experiments. Using the optimal hyperplane separation principle, we predicted individual and categorical indicator correlations. The results revealed significant correlations among specific autophagy-related cytokines: TGF-β1 showed a strong association with OCN, whereas PTH exhibited a significant correlation with OCN. Interestingly, IFN-γ demonstrated a positive correlation with PTH but a negative correlation with TGF-β1, suggesting that Tuina therapy for KOA may exert its therapeutic effects through the coordinated regulation of multiple autophagy-related cytokines via synergistic or antagonistic mechanisms.

Furthermore, our investigation identified strong correlations between four autophagy-related cytokines (TGF-β1, OCN, PTH, and IFN-γ) and both CAR and RAL indices, except for MMP-3, IL-17, and IL-1β. This pattern indicates that TGF-β1, OCN, PTH, and IFN-γ may play more prominent roles in mitigating cartilage degeneration and modulating cellular autophagy than other cytokines. Categorical correlation analysis demonstrated that cartilage degeneration exhibited the strongest association with autophagy-related cytokines and the weakest correlation with behavioral assessments. Moreover, a robust correlation was identified between autophagy and cartilage degeneration. Collectively, these findings suggest a critical tripartite relationship among autophagy-related cytokines, autophagy regulation, and cartilage degeneration. The regulation of autophagy-related cytokines to improve the level of autophagy and delay cartilage degeneration may be the key pathway of Tuina intervention in KOA.

ML methods were used to evaluate the recovery effect of Tuina and celecoxib on KOA. The results indicated that the overall effect of Tuina on KOA was superior to that of celecoxib, thereby highlighting that Tuina exhibited a stronger comprehensive ability to improve KOA-related indicators. In addition, the therapeutic effect of Tuina was confirmed based on the performance of each categorical feature. Tuina was superior to celecoxib in terms of behavioral metrics, cartilage degeneration, and autophagy-related cytokine levels. Comprehensive analyses revealed that the efficacy of the

ML model was consistent with that of animal experiments. The ML study affirmed the rationality of the metrics selected for the in vivo rat experiment and confirmed the results obtained.

This study established a comprehensive framework that synergistically integrates genetics, experimental validation, and computational predictions to form a robust evidentiary chain for the multidimensional verification of research outcomes. The organic convergence of these three approaches constructs a closed-loop research paradigm encompassing "genetic target discovery–biological functional validation–systemic mechanism elucidation". This integration highlights the methodological superiority of multidisciplinary convergence in unraveling the intricate mechanisms of Tuina therapy while providing a quantifiable analytical framework to systematically investigate the mechanisms by which Tuina regulates autophagy-related cytokines to improve autophagy and thus delay cartilage degeneration.

Conclusion

Collectively, Tuina therapy ameliorates KOA progression in rat models by modulating the expression of autophagy-related cytokines to suppress excessive chondrocyte autophagy, thereby reducing articular cartilage degeneration and enhancing chondrocyte repair capacity. To advance translational applications, future investigations should prioritize clinical validation studies to translate these preclinical findings into optimized therapeutic protocols for KOA management in humans.

Data Sharing Statement

The datasets used and/or analyzed during the current study are available from the corresponding author on reasonable request.

Ethics Approval and Consent to Participate

This study was approved by the Ethics Committee of Henan University of Traditional Chinese Medicine (Approval number: IACUC-202309024). All experiments were conducted in accordance with the National Institutes of Health's Guidelines for the Care and Use of Laboratory Animals.

Consent for Publication

All authors consent to publish this manuscript.

Author Contributions

Zhen Wang, Chi Zhao, Mengmeng Li and Lili Zhang have contributed equally to this work and share first authorship. All authors made a significant contribution to the work reported, whether that is in the conception, study design, execution, acquisition of data, analysis and interpretation, or in all these areas, took part in drafting, revising or critically reviewing the article, gave final approval of the version to be published; have agreed on the journal to which the article has been submitted; and agree to be accountable for all aspects of the work.

Funding

This work was supported by the Henan Province Chinese Medicine Scientific Research Special Project (No. 2024ZY3060, 2024ZY2096), the Henan Province Key Research Projects of Colleges and Universities (No. 26B360011), the Henan Province Chinese Medicine Research Special Project (Joint Construction) (2025LHZX3008), the Central Plains Thousand Talents Program-Central Plains Famous Doctors (No. ZYQR201912120), the 2022 Central Plains Talent Plan (Talent Education Series)-Central Plains Youth Top Talent Project (No. Yu Talent Office [2022] No. 5), the Henan Provincial International Science and Technology Cooperation Project (No. 252102521021), the Henan Provincial Science and Technology Research and Development Program (Joint Fund Project) (No. 242301420104), Henan Provincial Science and Technology Research and Development Plan Joint Fund Project (No. 222301420083), Henan Province Key Research and Development and Promotion Special Project (Science and Technology Research) (No. 232102311203), Henan Province Traditional Chinese Medicine "Double First-Class" Scientific Research Project (No. HSRP-DFCTCM-2023-7-09) and Henan University of Chinese Medicine Graduate Research Innovation Ability Improvement Plan Project (No. 2023KYCX071).

Disclosure

The authors declare no competing interests.

References

1. Giorgino R, Albano D, Fusco S, Peretti GM, Mangiavini L, Messina C. Knee osteoarthritis: epidemiology, pathogenesis, and mesenchymal stem cells: what else is new? An update. *Int J Mol Sci*. 2023;24(7):6405. doi:10.3390/ijms24076405
2. Liew JW, King LK, Mahmoudian A, et al. OARSI early osteoarthritis classification criteria task force. A scoping review of how early-stage knee osteoarthritis has been defined. *Osteoarthr Cartil*. 2023;31(9):1234–1241. doi:10.1016/j.joca.2023.04.015
3. Michael JW, Schlüter-Brust KU, Eysel P. The epidemiology, etiology, diagnosis, and treatment of osteoarthritis of the knee. *Dtsch Arztebl Int*. 2010;107(9):152–162. doi:10.3238/arztebl.2010.0152
4. Kan HS, Chan PK, Chiu KY, et al. Non-surgical treatment of knee osteoarthritis. *Hong Kong Med J*. 2019;25(2):127–133. doi:10.12809/hkmj187600
5. Hussain SM, Neilly DW, Baliga S, Patil S, Meek R. Knee osteoarthritis: a review of management options. *Scott Med J*. 2016;61(1):7–16. doi:10.1177/0036933015619588
6. Perruccio AV, Young JJ, Wilfong JM, Denise Power J, Canizares M, Badley EM. Osteoarthritis year in review 2023: epidemiology & therapy. *Osteoarthr Cartil*. 2024;32(2):159–165. doi:10.1016/j.joca.2023.11.012
7. Poenaru D, Sandulescu MI, Potcovaru CG, Cinteza D. High-intensity laser therapy in pain management of knee osteoarthritis. *Biomedicines*. 2024;12(8):1679. doi:10.3390/biomedicines12081679
8. Poenaru D, Sandulescu MI, Cinteza D. Pain modulation in chronic musculoskeletal disorders: botulinum toxin, a descriptive analysis. *Biomedicines*. 2023;11(7):1888. doi:10.3390/biomedicines11071888
9. Cao P, Li Y, Tang Y, Ding C, Hunter DJ. Pharmacotherapy for knee osteoarthritis: current and emerging therapies. *Expert Opin Pharmacother*. 2020;21(7):797–809. doi:10.1080/14656566.2020.1732924
10. Zhang H, Ge G, Zhang W, et al. PP2Ac regulates autophagy via mediating mTORC1 and ULK1 during osteoclastogenesis in the subchondral bone of osteoarthritis. *Adv Sci*. 2024;11(36):e2404080. doi:10.1002/advs.202404080
11. Lee JS, Kim YH, Jhun J, et al. Oxidized LDL accelerates cartilage destruction and inflammatory chondrocyte death in osteoarthritis by disrupting the TFEB-regulated autophagy-lysosome pathway. *Immune Netw*. 2024;24(3):e15. doi:10.4110/in.2024.24.e15
12. Xu K, He Y, Moqbel SAA, Zhou X, Wu L, Bao J. SIRT3 ameliorates osteoarthritis via regulating chondrocyte autophagy and apoptosis through the PI3K/Akt/mTOR pathway. *Int J Biol Macromol*. 2021;175:351–360. doi:10.1016/j.ijbiomac.2021.02.029
13. Kurakazu I, Akasaki Y, Tsushima H, et al. TGFβ1 signaling protects chondrocytes against oxidative stress via FOXO1-autophagy axis. *Osteoarthr Cartil*. 2021;29(11):1600–1613. doi:10.1016/j.joca.2021.07.015
14. Jiang J, Li J, Xiong C, Zhou X, Liu T. Isorhynchophylline alleviates cartilage degeneration in osteoarthritis by activating autophagy of chondrocytes. *J Orthop Surg Res*. 2023;18(1):154. doi:10.1186/s13018-023-03645-4
15. Liu K, Zhan Y, Zhang Y, et al. Efficacy and safety of Tuina (Chinese Therapeutic Massage) for knee osteoarthritis: a randomized, controlled, and crossover design clinical trial. *Front Med*. 2023;10:997116. doi:10.3389/fmed.2023.997116
16. Wang Z, Xu H, Wang Z, et al. Effects of externally-applied, non-pharmacological interventions on short- and long-term symptoms and inflammatory cytokine levels in patients with knee osteoarthritis: a systematic review and network meta-analysis. *Front Immunol*. 2023;14:1309751. doi:10.3389/fimmu.2023.1309751
17. Xu H, Zhao C, Guo G, et al. The effectiveness of tuina in relieving pain, negative emotions, and disability in knee osteoarthritis: a randomized controlled trial. *Pain Med*. 2023;24(3):244–257. doi:10.1093/pm/pnac127
18. Xu H, Xie J, Xiao LB, et al. Clinical observation on joint treatment of pain of knee osteoarthritis with local acupoint and sitting position. *World Sci Tech Modernization of Tradit Chin Med*. 2021;23(06):2125–2131.
19. Xu H, Kang BX, Zhong S, et al. Joint treatment of knee osteoarthritis with local acupoints and sitting position: a randomized controlled study. *J Tissue Eng*. 2021;25(02):216–221.
20. Zheng LJ, Wang K, Li MZ, Wang JM, Qiao YJ, Li HD. Shutiaojing massage can maintain the stability of the internal environment of rabbit cartilage cells damaged by knee osteoarthritis. *J Tissue Eng*. 2023;27(35):5681–5687.
21. Liang SM, Xu Y, Xie X-F. A study on the effects of "Shu Jin" manipulation on TNF-α, MMP-3, TIMP-1 and TGF-β1 in joint fluid of rabbits with knee osteoarthritis based on the theory of "tendon for bone". *Chengdu Univ Tradit Chin Med*. 2021;16:12–23. doi:10.26988/d.cnki.gcdzu.2021.000339
22. Estrada S, Arancibia M, Stojanova J, Papuzinski C. General concepts in biostatistics and clinical epidemiology: experimental studies with randomized clinical trial design. *Medwave*. 2020;20(3):e7869. doi:10.5867/medwave.2020.02.7869
23. Bensa A, Salerno M, Boffa A, et al. Corticosteroid injections for the treatment of osteoarthritis present a wide spectrum of effects ranging from detrimental to disease-modifying: a systematic review of preclinical evidence by the ESSKA orthobiologic initiative. *Knee Surg Sports Traumatol Arthrosc*. 2024;32(11):2725–2745. doi:10.1002/ksa.12242
24. Ference BA, Holmes MV, Smith GD. Using Mendelian randomization to improve the design of randomized trials. *Cold Spring Harb Perspect Med*. 2021;11(7):a040980. doi:10.1101/cshperspect.a040980
25. Grau-Perez M, Agha G, Pang Y, Bermudez JD, Tellez-Plaza M. Mendelian randomization and the environmental epigenetics of health: a systematic review. *Curr Environ Health Rep*. 2019;6(1):38–51. doi:10.1007/s40572-019-0226-3
26. Burgess S, Scott RA, Timpson NJ, Davey Smith G, Thompson SG. EPIC- InterAct consortium. Using published data in Mendelian randomization: a blueprint for efficient identification of causal risk factors. *Eur J Epidemiol*. 2015;30(7):543–552. doi:10.1007/s10654-015-0011-z
27. Handelman GS, Kok HK, Chandra RV, Razavi AH, Lee MJ, Asadi H. eDoctor: machine learning and the future of medicine. *J Intern Med*. 2018;284(6):603–619. doi:10.1111/joim.12822
28. Rauschert S, Raubenheimer K, Melton PE, Huang RC. Machine learning and clinical epigenetics: a review of challenges for diagnosis and classification. *Clin Epigenetics*. 2020;12(1):51. doi:10.1186/s13148-020-00842-4
29. Allman PH, Aban IB, Tiwari HK, Cutter GR. An introduction to Mendelian randomization with applications in neurology. *Mult Scler Relat Disord*. 2018;24:72–78. doi:10.1016/j.msard.2018.06.017

30. Weng H, Li H, Zhang Z, et al. Association between uric acid and risk of venous thromboembolism in East Asian populations: a cohort and Mendelian randomization study. *Lancet Reg Health West Pac*. 2023;39:100848. doi:10.1016/j.lanwpc.2023.100848
31. Ho J, Mak CCH, Sharma V, To K, Khan W. Mendelian Randomization Studies of Lifestyle-Related Risk Factors for Osteoarthritis: a PRISMA Review and Meta-Analysis. *Int J Mol Sci*. 2022;23(19):11906. doi:10.3390/ijms231911906
32. Wang Z, Zhao C, Wang Z, et al. Elucidating causal relationships among gut microbiota, human blood metabolites, and knee osteoarthritis: evidence from a two-stage mendelian randomization analysis. *Rejuvenation Res*. 2025. doi:10.1089/rej.2024.0079
33. Su Y, Xu S, Ma Y, et al. A modified debiased inverse-variance weighted estimator in two-sample summary-data Mendelian randomization. *Stat Med*. 2024;43(29):5484–5496. doi:10.1002/sim.10245
34. Burgess S, Thompson SG. Interpreting findings from Mendelian randomization using the MR-Egger method. *Eur J Epidemiol*. 2017;32 (5):377–389. doi:10.1007/s10654-017-0255-x
35. Xu J, Zhang S, Tian Y, et al. Genetic causal association between iron status and osteoarthritis: a two-sample Mendelian randomization. *Nutrients*. 2022;14(18):3683. doi:10.3390/nu14183683
36. Gupta V, Walia GK, Sachdeva MP. 'Mendelian randomization': an approach for exploring causal relations in epidemiology. *Public Health*. 2017;145:113–119. doi:10.1016/j.puhe.2016.12.033
37. Carter AR, Sanderson E, Hammerton G, et al. Mendelian randomisation for mediation analysis: current methods and challenges for implementation. *Eur J Epidemiol*. 2021;36(5):465–478. doi:10.1007/s10654-021-00757-1
38. Yao N, Chen GC, Lu YY, et al. Bushen Qiangjin capsule inhibits the Wnt/α-catenin pathway to ameliorate papain-induced knee osteoarthritis in rat. *J Tradit Chin Med*. 2021;41(6):935–942. doi:10.19852/j.cnki.jtcm
39. Cheng F, Yan FF, Liu YP, Cong Y, Sun KF, He XM. Dexmedetomidine inhibits the NF-κB pathway and NLRP3 inflammasome to attenuate papain-induced osteoarthritis in rats. *Pharm Biol*. 2019;57(1):649–659. doi:10.1080/13880209.2019.1651874
40. Wang Z, Xu H, Wang Z, et al. Traditional Chinese manual therapy (Tuina) improves knee osteoarthritis by regulating chondrocyte autophagy and apoptosis via the PI3K/AKT/mTOR pathway: an in vivo rat experiment and machine learning study. *J Inflamm Res*. 2024;17:6501–6519. doi:10.2147/JIR.S488023
41. Abdelfattah S, Baza M, Mahmoud M, et al. Lightweight multi-class support vector machine-based medical diagnosis system with privacy preservation. *Sensors*. 2023;23(22):9033. doi:10.3390/s23229033
42. Luan T, Yang X, Kuang G, et al. Identification and analysis of neutrophil extracellular trap-related genes in osteoarthritis by bioinformatics and experimental verification. *J Inflamm Res*. 2023;16:3837–3852. doi:10.2147/JIR.S414452
43. Bertoncelli CM, Altamura P, Bagui S, et al. Predicting osteoarthritis in adults using statistical data mining and machine learning. *Ther Adv Musculoskelet Dis*. 2022;14:1759720X221104935. doi:10.1177/1759720X221104935
44. Pushpa B, Baskaran B, Vivekanandan S, Gokul P. Liver fat analysis using optimized support vector machine with support vector regression. *Technol Health Care*. 2023;31(3):867–886. doi:10.3233/THC-220254
45. Cardozo G, Pintarelli GB, Andreis GR, Lopes ACW, Marques JLB. Use of machine learning and routine laboratory tests for diabetes mellitus screening. *Biomed Res Int*. 2022;2022:8114049. doi:10.1155/2022/8114049
46. Chicco D, Warrens MJ, Jurman G. The coefficient of determination R-squared is more informative than SMAPE, MAE, MAPE, MSE and RMSE in regression analysis evaluation. *PeerJ Comput Sci*. 2021;7:e623. doi:10.7717/peerj-cs.623
47. Chen X, Gong W, Shao X, et al. METTL3-mediated m6A modification of ATG7 regulates autophagy-GATA4 axis to promote cellular senescence and osteoarthritis progression. *Ann Rheum Dis*. 2022;81(1):87–99. doi:10.1136/annrheumdis-2021-221091
48. Wang FS, Kuo CW, Ko JY, et al. Irisin mitigates oxidative stress, chondrocyte dysfunction and osteoarthritis development through regulating mitochondrial integrity and autophagy. *Antioxidants*. 2020;9(9):810. doi:10.3390/antiox9090810
49. Li M, Peng Z, Wang X, Wang Y. Monoamine oxidase A attenuates chondrocyte loss and extracellular matrix degradation in osteoarthritis by inducing autophagy. *Int Immunopharmacol*. 2022;109:108772. doi:10.1016/j.intimp.2022.108772
50. Lv X, Zhao T, Dai Y, et al. New insights into the interplay between autophagy and cartilage degeneration in osteoarthritis. *Front Cell Dev Biol*. 2022;10:1089668. doi:10.3389/fcell.2022.1089668
51. Chen S, Saeed AFUH, Liu Q, et al. Macrophages in immunoregulation and therapeutics. *Signal Transduct Target Ther*. 2023;8(1):207. doi:10.1038/s41392-023-01452-1
52. Kostrzewa-Nowak D, Trzeciak-Ryczek A, Wityk P, Cembrowska-Lech D, Nowak R. Post-effort changes in autophagy- and inflammation-related gene expression in white blood cells of healthy young men. *Cells*. 2021;10(6):1406. doi:10.3390/cells10061406
53. Gulisaal E, Liu JC, Wang YF, et al. Effects of Chenyuan plaster treatment on apoptosis, matrix metalloproteinase and serum inflammatory factors of articular chondrocytes in rabbit model of knee osteoarthritis with Yang deficiency and cold coagulation. *J Tradit Chin Med*. 2022;63 (22):2154–2161.
54. Chen GS, Zhan GP, Wu BB. Clinical study of warm acupuncture combined with Tuina for treatment of knee osteoarthritis. *New Chinese Medicine*. 2023;55(09):183–186.
55. Sekula P, Del Greco MF, Pattaro C, Köttgen A. Mendelian randomization as an approach to assess causality using observational data. *J Am Soc Nephrol*. 2016;27(11):3253–3265. doi:10.1681/ASN.2016010098
56. Zhang XL, Huang ZY, Xing HH, et al. Research progress of animal selection for modeling of knee osteoarthritis. *J Hubei Med Univ*. 2019;44(01):107–113.
57. Ye JS, Liang ZC. Comparison of three different methods of knee osteoarthritis modeling. *Chin J Gerontol*. 2019;43(16):3948–3954.
58. Jin X, Yu Y, Lin Y, Yang J, Chen Z. Tendon-regulating and bone-setting manipulation promotes the recovery of synovial inflammation in rabbits with knee osteoarthritis via the TLR4-MyD88-NF-κB signaling pathway. *Ann Transl Med*. 2023;11(6):245. doi:10.21037/atm-22-3039
59. Yang N, Zuo J, Yang GQ, Bi YF. Research progress of traditional Chinese medicine in treatment of knee osteoarthritis. *Yunnan J Tradit Chin Med*. 2016;37(11):92–93.
60. Kang ZR, Gong L, Xing H, Dai DC. A preliminary study on the therapeutic concept and principle of sitting knee adjustment in the treatment of knee osteoarthritis. *J Shanghai Univ Tradit Chin Med*. 2020;34(04):98–102.
61. Mora JC, Przkora R, Cruz-Almeida Y. Knee osteoarthritis: pathophysiology and current treatment modalities. *J Pain Res*. 2018;11:2189–2196. doi:10.2147/JPR.S154002
62. Rutgers M, Saris DB, Yang KG, Dhert WJ, Creemers LB. Joint injury and osteoarthritis: soluble mediators in the course and treatment of cartilage pathology. *Immunotherapy*. 2009;1(3):435–445. doi:10.2217/imt.09.14